Adaptive Space/Frequency Processing for Distributed Aperture Radars

Raviraj Adve[a], Richard Schneible[b], Robert McMillan[c]
[a]University of Toronto
Department of Electrical and Computer Engineering
10 King's College Road
Toronto, ON M5S 3G4 Canada
[b]Stiefvater Consultants
10002 Hillside Terrace
Marcy, NY 13403, USA
[c] US Army SMDC
Huntsville, AL 35805, USA

Abstract- This paper details a preliminary investigation into space-time-waveform adaptive processing for waveform diverse distributed apertures. The large baseline of such a distributed radar results in angular resolution that is orders of magnitude better than the resolution of a monolithic system (single large radar) with the same power-aperture. This capability comes at the cost of grating lobes (multistatics with evenly spaced apertures) or high sidelobes (multistatics with randomly spaced apertures). This paper develops some preliminary solutions to these drawbacks associated with distributed apertures. In particular, the use of approximately logarithmic spacing with each aperture transmitting orthogonal waveforms provides excellent detection performance.

I. INTRODUCTION

This paper investigates the application of adaptive processing to a relatively new concept in radar systems: waveform diverse distributed apertures. In such a radar, the transmit/receive aperture is divided into a number of subapertures that can be placed in various locations relative to each other. The distributed radar operates in a multistatic mode with all apertures transmitting (either the same signal, different uncorrelated signals or orthogonal signals). Multistatic radars can provide significantly improved target tracking and interference rejection because of the large baseline between the various apertures. The large baseline results in angular resolution that is orders of magnitude better than the resolution of a monolithic system (single large radar) with the same power-aperture. This capability comes at the cost of grating lobes (multistatics with evenly spaced apertures) or high sidelobes (multistatics with randomly spaced apertures).

In a related paper, we have shown that a new mode of multistatic operation is required to achieve the improved interference rejection while maintaining the systems' surveillance capability. In this mode, the subapertures radiate mutually orthogonal waveforms, however, each subaperture receives and processes all orthogonal waveforms. Consider a distributed aperture with N subapertures. Since each subaperture receives the returns form all transmitted waveforms, there are $N \times N$ returned signals for each radar range. A space-waveform-range data cube therefore replaces the usual space-time-range data cube. In this paper, the orthogonal waveforms are chosen to be relatively narrowband signals offset in center frequency. Here we report on the use of *optimal adaptive* space/waveform processing for such a distributed aperture. In particular, we compare this situation to the traditional case where subapertures transmit the same waveform.

In such a system, there are a few unique concepts:

- Adaptive space/waveform processing: Traditionally, adaptive processing has focused on the space and time dimensions leading to space-time adaptive processing (STAP). The spatial steering vector is related to the look direction while the temporal steering vector is determined by the look Doppler frequency. In our case, the time dimension is replaced with the *waveform* dimension. The space/waveform steering vector is determined by the look angle uniquely with a different spatial steering vector for each transmit frequency.
- Spacing of subapertures/waveforms (frequencies): Distributing the apertures and separating the transmit frequencies introduces two new degrees of freedom available to the radar designer: the spacing between the antenna elements and the frequencies. Equally spaced elements with equally spaced frequencies can lead to grating lobes that can reduce the effectiveness of the adaptive process. Here we investigate various configurations, comparing them in terms of grating lobes, mainbeam width, etc. Future work will investigate the optimization of these parameters with respect to some performance measures.
- Targets/interference are not necessarily in the far field: By common definition, the fair field region is determined by three conditions: $R > \lambda$, $R > D$ and $R > D^2/\lambda$ where R is the radial distance, D is the *total* aperture baseline and λ is the frequency of operation [1]. From a physical point of view, the far field may be defined as the region where the spatial steering vector is effectively

independent of the radial distance. In our example, we choose D = 200m with a center frequency 10GHz, setting the beginning of the far field at approximately 1500km. The target and interference are therefore not necessarily in the far field. This has serious implications in the type of adaptive processing scheme chosen, including choice of secondary data to estimate the interference covariance matrix. Similar to STAP for bistatic radar, this range dependent steering vector reduces the secondary data available to estimate the covariance matrix.[2, 3].

In addition to the above, another important consideration is position errors in the array. Due to the large baseline, a relatively small error in position may be comparable to the wavelength of operation. This is especially true for radars operating at X-band.

Section II describes the system model and the adaptive processing scheme. Section III presents some preliminary results for space-time-waveform adaptive processing for waveform diverse distributed apertures. Finally, Section IV presents some conclusions and points to some future work.

II. SYSTEM MODEL AND ADAPTIVE PROCESSING SCHEME

The elements of the linear array are not equally spaced and each element in the array may transmits at a frequency. Let $\{x_n$, n = 0,1,2…N-1$\}$ denote the positions of the N elements, each with corresponding frequency $\{f_n$, n = 0,1,2…N-1$\}$. Each element receives and processes the signals from all N transmissions. Consider a scenario wherein each element transmits M pulses within a single coherent pulse interval (CPI) at a pulse repetition frequency (PRF) of f_r. Due to these N transmissions, the return signal from a unit target at the n^{th} element, k^{th} frequency and m^{th} pulse, for a target at relative velocity v and relative angle φ is given by

$$s(n,k,m) = \exp\left(j2\pi m \frac{f_{dk}}{f_r} \right) \exp\left(j \frac{2\pi x_n f_k \sin\varphi}{c} \right), \quad (1)$$

where f_{dk} is the Doppler frequency associated with transmit frequency f_k, i.e.

$$f_{dk} = \frac{2 v f_k}{c}, \quad (2)$$

$$s(n,k,m) = \exp\left(j2\pi m \frac{2 v f_k}{c f_r} \right) \exp\left(j \frac{2\pi x_n f_k \sin\varphi}{c} \right). \quad (3)$$

This signal can be written as a length N^2M *space-waveform-time* steering vector

$$\mathbf{s}(v,\varphi) = \left[\mathbf{s}_0^T \;\; \mathbf{s}_1^T \;\; \mathbf{s}_2^T \;\; \ldots \mathbf{s}_k^T \;\; \ldots \;\; \mathbf{s}_{N-1}^T \right]^T, \quad (4)$$

where each length NM vector, $\mathbf{s}_k$ is the traditional space-time steering vector for center frequency f_k

$$\mathbf{s}_k = \mathbf{b}_k(v) \otimes \mathbf{a}_k(\varphi), \quad (5)$$

$$\mathbf{b}_k(v) = \begin{bmatrix} 1 \\ \exp\left(j2\pi \frac{2 v f_k}{c f_r} \right) \\ \vdots \\ \exp\left(j2\pi (M-1) \frac{2 v f_k}{c f_r} \right) \end{bmatrix}, \quad (6)$$

$$\mathbf{a}_k(\varphi) = \begin{bmatrix} 1 \\ \exp\left(j \frac{2\pi x_1 f_k \sin\varphi}{c} \right) \\ \vdots \\ \exp\left(j \frac{2\pi x_{N-1} f_k \sin\varphi}{c} \right) \end{bmatrix}. \quad (7)$$

Note that both the spatial and temporal steering vectors are defined in terms of the N frequencies of operation f_k. Also, unlike the traditional spatial steering vector for a linear equi-spaced array, the spatial steering vector here is defined in terms of the position of the elements x_k.

The jammer signal has a structure similar to the target signal. Here we model Gaussian barrage noise jammers. Hence, the only difference between the target and jammer models is that the temporal steering vector is replaced by a vector of independent, complex, Gaussian random variables. The jammer signal, for frequency index k is modeled as

$$\mathbf{s}_{Jk} = \xi_{Jk} \, \mathbf{b}_{Jk} \otimes \mathbf{a}_k(\varphi_J), \quad (8)$$

where ξ_{Jk} is the amplitude of the jammer and the temporal vector $\mathbf{b}_J$ is a white, complex Gaussian random vector of independent random variables with zero mean and unit variance. The length N^2M vector of jammer signal is therefore

$$\mathbf{s}_J = \left[\mathbf{s}_{J0}^T \;\; \mathbf{s}_{J1}^T \;\; \mathbf{s}_{J2}^T \;\; \ldots \mathbf{s}_{Jk}^T \;\; \ldots \;\; \mathbf{s}_{J(N-1)}^T \right]^T, \quad (9)$$

Noise is modeled as a white complex Gaussian random variable for all frequencies, pulses and elements. The overall received signal, is therefore given by,

$$\mathbf{x} = \xi_t \mathbf{s}(v,\varphi) + \mathbf{s}_J + \mathbf{n}, \quad (10)$$

where $\mathbf{n}$ is complex Gaussian noise vector.

Using the signal in Eqn. (10), we can now implement a space-time-waveform adaptive processing algorithm. The algorithm chosen here is the traditional optimal approach where the N^2M elements of the received signal $\mathbf{x}$ are combined using a weight vector $\mathbf{w}$. The weight vector is determined using the relation

$$\mathbf{w} = \mathbf{R}^{-1}\mathbf{s}, \quad (11)$$

where $\mathbf{s}$ is the space-time-waveform steering vector of Eqn. (4) and $\mathbf{R}$ is the interference plus noise covariance matrix. Note that in practice, this matrix must be estimated.

A. Data Generation and Implementation of Adaptive Process

Using Eqn. (10) above, received data can be generated corresponding to the chosen scenario. Repeating this several times, e.g. (P+1) times, yields a space-time-waveform-range hypercube, organized as a $N^2M \times (P + 1)$ matrix. Each column of this matrix corresponds to a single range. To implement an adaptive process, using this data, a space-time-waveform covariance matrix is estimated.

In the simulations presented in Section III, the data for the (P + 1) ranges is generated without a target, i.e. $\xi_t = 0$. Then a target with chosen power is injected into the middle range, p = (P/2+1). For the q^{th} range, an interference covariance matrix is estimated by using a sliding window

$$\hat{\mathbf{R}} = \sum_{\substack{p=1 \\ p \neq q}}^{P+1} \mathbf{x}_p \mathbf{x}_p^H \quad , \tag{12}$$

where the superscript ^{H} represents the Hermitian of a complex matrix and $\mathbf{x}_p$ represents one of (P+1) snapshots of data. In general, for a reasonably accurate estimate of $\mathbf{R}$, we need $P > 2N^2M$ [4]. The adaptive weights are obtained using Eqn. (11). Using these weights we define the modified sample matrix inversion (MSMI) statistic, which as the property of having constant false alarm rate (CFAR) in Gaussian interference,

$$\rho_p = \frac{\left|\mathbf{w}^H \mathbf{x}_p\right|^2}{\left|\mathbf{w}^H \mathbf{s}(v,\varphi)\right|^2} \, . \tag{13}$$

This statistic is plotted as a function of range. Clearly, if the range corresponds to the one with the target, the output statistic should be as large as possible, while if the range does not contain a target, the output MSMI statistic should be close to zero.

These weights are also used to obtain the output signal-to-jammer-ratio (SJR), assuming a unit target, as

$$SJR = \frac{\mathbf{w}^H \mathbf{s}(v,\varphi)}{\mathbf{w}^H \mathbf{s}_{\mathrm{J}}} \, . \tag{14}$$

Note that the jammer signal $\mathbf{s}_{\mathrm{J}}$ includes the jammer amplitude. In this analysis, to illustrate jammer suppression, this SJR is plotted as a function of jammer angle φ.

III. PRELIMINARY RESULTS

Unless stated otherwise, the parameters chosen in the test scenarios are given in Table 1.

Table 1: Parameters for test scenario

N	6	PRF	2kHz
Center Frequency	10GHz	Jammer-to-Noise Ratio	50dB
Frequency Offset	100MHz	Target SNR	0dB
Radar Baseline	200m	Target velocity (v)	10m/s
Pulses in CPI (M)	12	Number of range bins (P + 1)	1728

The frequency offset given in Table 1 is used in the case where different elements transmit on different frequencies. When using the frequency offset, each transmission is separated by 100MHz. The first null beam width of such an array is 0.014°.

A. Statistic Versus Range

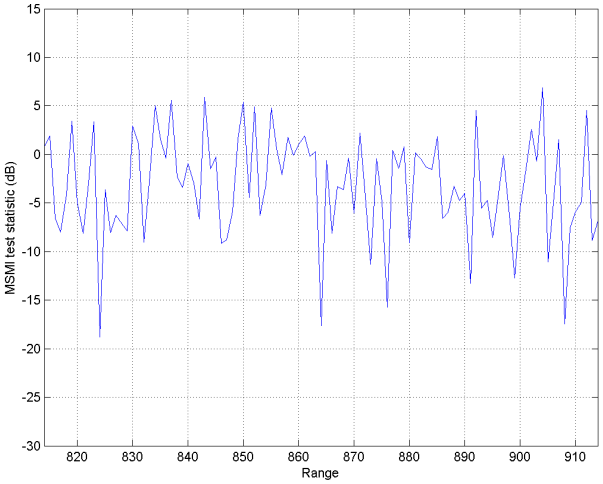

Figure 1: MSMI statistic versus range. No frequency offsets.

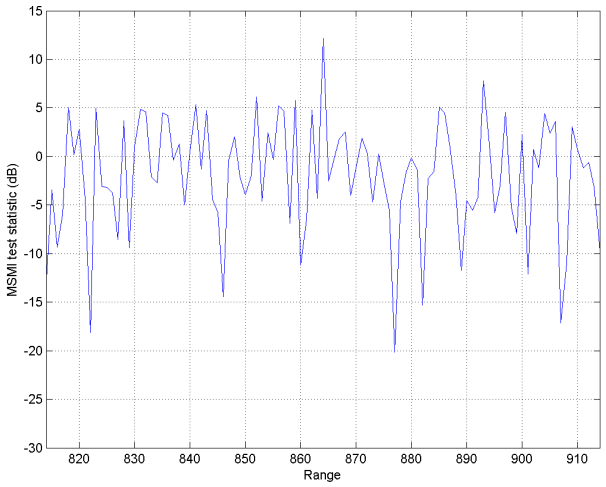

Figure 2: MSMI statistic versus range. Using frequency offsets (orthogonal waveforms)

The first example illustrates the use of orthogonal waveforms to separate target from interference. The target is at broadside in range bin 865. A 50dB barrage noise jammer at 0.04297^{o}, approximately three first-null beamwidths away, hinders target detection. Figure 1 and Figure 2 plot the MSMI statistic versus range for two cases considered here: in Figure 1, all six elements transmit at the same frequency whereas, in Figure 2, each element transmits orthogonal waveforms (waveforms separated in center frequency by 100MHz). Both figures plot the MSMI test statistic versus range close to the range cell where the target was injected. As is clear from the figures, when all elements transmit at the same frequency, the target cannot be distinguished from the interference. Whereas, when each element transmits a orthogonal waveforms (different frequencies), the target is clearly visible, with approximately a 6dB separation between target and interference.

The rest of the examples plot the output signal-to-jammer ratio (SJR) versus jammer angle.

B. SJR versus Jammer Angle. Equally Spaced Elements

The second example, again, compares the use of the same frequency from each element with using multiple frequencies (orthogonal waveforms). The elements of the array are equally spaced. The jammers are stepped over angles spaced by 1.4×10^{-3} degrees. This example uses only one pulse, i.e. $M = 1$.

Figure 3 plots the output SJR versus angle for the case where all elements transmit at the same frequency. The output SJR is rather high for most angles. However, at certain angles for the jammer, the SJR shows deep nulls as the null in direction of target. The large null at the target look direction is expected as the jammer and target cannot be at the same location. The deep nulls in the other directions are due to the grating lobes associated with equal spacing and all elements transmitting at the same frequency.

Figure 4 plots the SJR for the case where each element transmits at a different frequency. The deep null at the target is visible, however, clearly there is a huge improvement in grating lobes. Off-target nulls still occur, the nulls are much shallower and much further away from the target location. To confirm the fact that grating lobes are reduced in this case, in Figure 4, the analysis is conducted over a much larger angular extent than in Figure 3. The resolution, however, is the same. Note that the off-target nulls in Figure 4 are broader than the off-target nulls in Figure 3, i.e. while using multiple frequencies helps, the off-target nulls broaden. This is true due to the equal spacing between array elements.

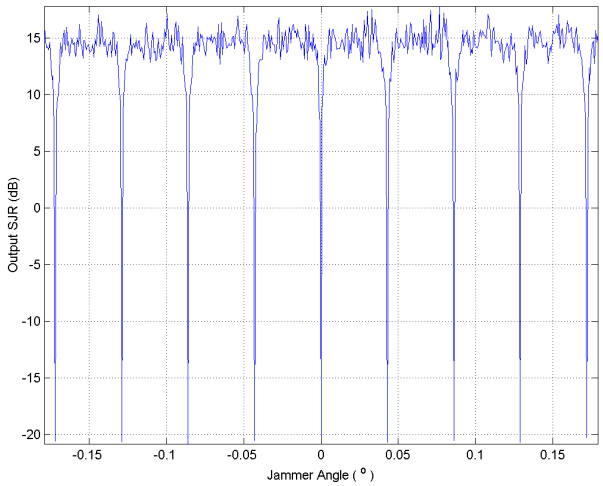

Figure 3: Signal-to-jammer ratio. Equal frequencies and element spacing.

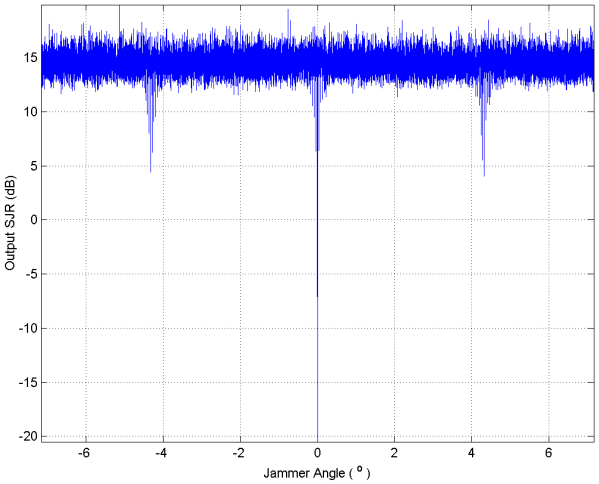

Figure 4: Signal to jammer ratio versus jammer angle.

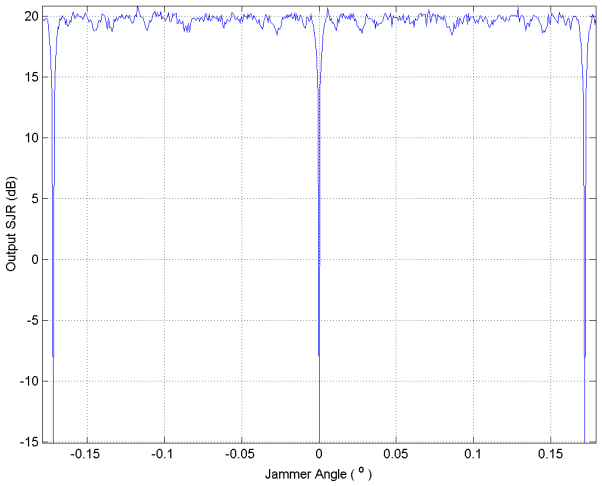

Figure 5: Signal-to-jammer ratio. Log spacing and the same frequency.

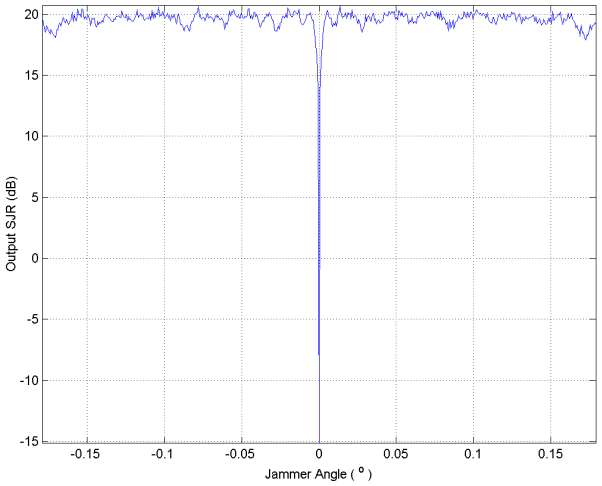

Figure 6: Signal to jammer ratio. Log spacing and orthogonal waveforms.

The next example illustrates the use of unequal spacing, here close to log-spacing. The six elements are located at *0m, 20m, 60m, 140m, 190m and 200m*. Figure 5 plots the output SJR versus jammer angle for the case where all elements transmit at the same frequency. In comparing with Figure 3, clearly the grating lobes are significantly reduced in number. However, note that there still exist grating lobes that are spaced further away. Figure 6 plots the SJR for the case of using orthogonal waveforms (unequal frequencies). Here the grating lobes are totally eliminated and the output SJR is high, except at extremely close to the target look direction. The null is less than 1.4×10^{-3} degrees wide.

IV. CONCLUSIONS AND EXTENSIONS

This paper has documented a preliminary investigation into the use of waveform diverse distributed apertures. The use of diverse waveforms, in the form of frequency offset orthogonal signals, overcomes a significant drawback with distributed apertures, i.e. grating lobes. By choosing an approximately logarithmic spacing, coupled with frequency diverse waveforms, grating lobes are eliminated.

The analysis here is undertaken under ideal conditions. The most important extension would be to include range dependent target and jamming signals. The extremely long radar baseline sets the beginning of the far field beyond any practical ranges. Similar to bistatic radar, the range dependent data would reduce the secondary data available to accurately estimate an interference covariance matrix. This issue leads to another possible extension, namely the development of new adaptive processing schemes specifically for waveform diverse distributed apertures.

ACKNOWLEDGMENTS

This effort was supported in part by US Army SMDC under contract DASGO-02-R-0037.

REFERENCES

[1] Balanis, C., *Antenna Theory, Analysis and Design*: John Wiley 1997.

[2] Himed, B., J.H. Michels, Y. Zhang. *Bistatic STAP performance analysis in radar applications*. in Proceedings of the *2001 IEEE Radar Conference*. pp. 198-203, 2001. Atlanta, GA.

[3] Sanyal, P.K., R.D. Brown, M.O. Little, R.A. Schneible, M.C. Wicks,. *Space-time adaptive processing bistatic airborne radar*. in Proceedings of the *1999 IEEE Radar Conference*. pp. 1999. Waltham, MA.

[4] Ward, J., *Space-time adaptive processing for airborne radar*. Technical Report. 1994, MIT Lincoln Laboratory: Cambridge, MA.